Annealing-Based Quantum Computing for Combinatorial Optimal Power Flow

Thomas Morstyn, *Senior Member, IEEE*

***Abstract*—This paper proposes the use of annealing-based quantum computing for solving combinatorial optimal power flow problems. Quantum annealers provide a physical computing platform which utilises quantum phase transitions to solve specific classes of combinatorial problems. These devices have seen rapid increases in scale and performance, and are now approaching the point where they could be valuable for industrial applications. This paper shows how an optimal power flow problem incorporating linear multiphase network modelling, discrete sources of energy flexibility, renewable generation placement/sizing and network upgrade decisions can be formulated as a quadratic unconstrained binary optimisation problem, which can be solved by quantum annealing. Case studies with these components integrated with the IEEE European Low Voltage Test Feeder are implemented using D-Wave Systems' 5,760 qubit Advantage quantum processing unit and hybrid quantum-classical solver.**

***Index Terms*—Distribution network, D-Wave, electric vehicle, optimal power flow, power system planning, quantum annealing, quantum computing. smart charging.**

I. Introduction

THE OPTIMAL deployment and operation of new sources of generation and flexibility is critical for achieving a low-cost transition to reliable and decarbonised electrical power systems [1]. The scope for optimised planning and operation has expanded significantly due to the emergence of distributed energy resources (DERs), including small and medium scale renewables and flexible loads, combined with the new availability of substation- and customer-level sensing and communications [2]. However, the vast potential scale of the resulting coordination challenge has created concern over future computational requirements [3].

Optimal power flow (OPF) problems involve finding set-points for controllable power sources which meet demand at minimum cost, while satisfying resource and network constraints [4]. In general, the nonlinear characteristics of power networks makes this challenging, which has motivated the development of linear approximations [5] and convex relaxations [6], which are accurate under specific conditions and allow OPF problems to be solved in polynomial time. With the rise of DERs, there has been significant work to consider the particular features of OPF relevant at the distribution system level, including unbalanced voltages, losses and reactive power flows [7], [8], [9].

Combinatorial OPF is a more challenging class of problem, which emerges when an OPF needs to be solved alongside additional discrete decisions, such as when resources have discrete flexibility [10], as well as where resource placement and network investment decisions need to be made accounting for fixed costs and limited sizing options [11]. In practice, many DERs only offer flexibility in discrete increments, including EV chargers [12] and heat-pumps [13] with on/off control, and schedulable appliances with fixed operating cycles [14]. Also, even when power converters allow continuous control of DERs, low operating power is often associated with low efficiency, making it desirable to impose a minimum turn-on power [15]. Combinatorial OPF is directly relevant for distribution system operators (DSOs) seeking to increase the hosting capacity for clean energy technologies through a combination of targeted network reinforcements and active management of DERs [16].

Combinatorial optimisation problems can be solved using exhaustive search and dynamic programming, but the curse of dimensionality means that the computational burden increases exponentially with the number of decision variables [17]. Mixed Integer Linear Programming (MILP) can be applied in cases where the objective and constraints can be formulated as linear functions of the discrete variables [18]. Significant progress has been made towards solving large MILPs to reasonable levels of accuracy, but in general they remain computationally intensive [19]. Lagrangian Relaxation [20] and Surrogate Lagrangian Relaxation [21] are iterative approaches suited to problems that can be decomposed into a set of simpler subproblems by relaxing a limited number of coupling constraints. Combinatorial problems can also be solved using metaheuristic methods including genetic algorithms [22], particle swarm optimisation [23], tabu search [24] and simulated annealing [25]. However, scalability remains a challenge as the convergence time of metaheuristic methods also increases with the problem dimension [26].

Over the last 20 years, there has been significant progress in the development of quantum devices which offer a fundamentally new computing architecture compared with classical digital silicon-based computers. A major milestone towards

Manuscript received 17 February 2022; revised 10 June 2022 and 14 August 2022; accepted 17 August 2022. Date of publication 22 August 2022; date of current version 20 February 2023. This work was supported by the U.K. Engineering and Physical Sciences Research Council (EPSRC) under Project EP/S000887/2, Project EP/S031901/1, and Project EP/T028564/1. Paper no. TSG-00227-2022.

The author is with the School of Engineering, The University of Edinburgh, Edinburgh EH8 9YL, U.K. (e-mail: thomas.morstyn@ed.ac.uk).

Color versions of one or more figures in this article are available at https://doi.org/10.1109/TSG.2022.3200590.

Digital Object Identifier 10.1109/TSG.2022.3200590

this was the recent achievement of quantum supremacy with a 54-qubit device, i.e., the practical demonstration of a quantum computer solving a problem that would be infeasible for classical computers [27]. For power systems, gate-based quantum computing algorithms are presented for generator unit commitment in [28], [29]. However, significant challenges remain for scaling up universal gate-based quantum computers to the point where they could be widely used for industrial applications [30].

The challenges of scaling up gate-based quantum computers has motivated the development of more scalable quantum hardware architectures aimed at specific computing problems. Quantum annealers are currently the largest quantum computing devices and are capable of solving a specific class of combinatorial optimisation, namely unconstrained quadratic binary optimisation (QUBO) problems [31]. Quantum annealers incorporate a lattice of qubits which can be controllably biased and coupled. Based on the quantum adiabatic theorem, the qubit lattice is controlled so that it physically evolves to a low-energy state which represents the solution to an optimisation problem. This is somewhat analogous to the process that is replicated by simulated annealing, but with physical quantum fluctuations replacing simulated thermal ones [32]. Also, it should be noted that before the development of annealing-based quantum processors, quantum annealing was used to refer to a variation of simulated annealing with simulated quantum fluctuations [33].

Theoretically demonstrating when noisy quantum annealing has a definitive advantage over classical alternatives is challenging [34], but a performance advantage has been demonstrated for specific applications [35], [36]. Moreover, quantum annealing hardware is still in its infancy, and is rapidly improving in terms of the number of qubits and noise level [37]. This has motivated investigations into a range applications including protein folding [38], machine learning [39], and wireless base station decoding [40]. The opportunity for quantum annealing to be applied to power system applications is noted in [41], but without a detailed investigation. In [42], quantum annealing is demonstrated for generator unit commitment, but power flow modelling and network constraints are not considered. Other power system applications of quantum annealing include grid partitioning [43] and phasor measurement unit placement [44].

The novel contribution of this paper is to propose and demonstrate the use of annealing-based quantum computing for combinatorial OPF. Given the still relatively limited scale and developing nature of quantum annealing hardware, our focus is on its applicability to power systems rather than the potential for speed-up with current hardware. Towards this, a novel QUBO formulation is presented for a linear multiphase OPF problem with controllable on/off EV charging, non-dispatchable renewable generation placement/sizing and network upgrade decisions, which can be solved using quantum annealing. Case studies are implemented on D-Wave Systems' 5,760 qubit Advantage quantum processor to investigate how the number of required qubits scales with the number of EVs and network constraints. D-Wave's hybrid quantum-classical binary quadratic model solver is then used for a larger scale problem, which highlights the value of co-optimising distribution network upgrades and renewable generation investment with operational flexibility.

The rest of the paper is organised as follows: Section II presents a brief overview of D-Wave's implementation of quantum annealing and its application to QUBO problems. In Section III, the proposed QUBO formulation for the combinatorial OPF is developed. Case study results are presented in Section IV. Section V concludes the paper.

II. Quantum Annealing

This section provides an overview of quantum annealing, as implemented by D-Wave's quantum processors. As mentioned, a key application is to solve QUBO problems, which can be described by

$$\min \sum_{(i,j)\in\mathcal{E}} Q_{ij}x_i x_j + \sum_{i\in\mathcal{X}} c_i x_i, \tag{1}$$

where $x_i \in \{0,1\}, i \in \mathcal{X} := \{1,\ldots,X\}$ are binary decision variables, $\mathcal{E} := \{(i,j)|i,j \in \mathcal{X}, i \neq j\}$. $Q_{ij} \in \mathbb{R}, (i,j) \in \mathcal{E}$ are the quadratic QUBO objective function coefficients and $c_i \in \mathbb{R}, i \in \mathcal{X}$ are the linear QUBO objective function coefficients.

The QUBO problem can be equivalently expressed as an Ising model minimisation problem, through a change of variables $y_i = 1 - 2x_i$ for $i \in \mathcal{X}$ [31], giving

$$\min \sum_{(i,j)\in\mathcal{E}} J_{ij}y_i y_j + \sum_{i\in\mathcal{X}} h_i y_i,$$
$$J_{ij} = -\frac{1}{4}Q_{ij},\ \ h_i = -\frac{1}{2}\left(c_i + \sum_{j\in\mathcal{X}} Q_{ij}\right), \tag{2}$$

where the spin values $y_i \in \{-1,1\}, i \in \mathcal{X}$.

Quantum annealing is based on the natural behaviour of coupled qubits to seek a ground state (lowest-energy state). The quantum annealing process can be described by a time varying Hamiltonian $\mathcal{H}(s)$ [34]

$$\mathcal{H}(s) = A(s)H_I - B(s)H_P, \tag{3}$$

where $A(s)$ and $B(s)$ are annealing path functions, which are defined in terms of the normalised annealing time $s = t/t_a$. These are designed so that initially $A(0) = 1$ and $B(0) = 0$, and after annealing $A(1) = 0$ and $B(1) = 1$.

The initial Hamiltonian H_I is selected so that it has a known ground state which is easy to prepare, for example [34]

$$H_I = \sum_i \sigma_i^x, \tag{4}$$

where σ_i^x is the Pauli-x operator applied to qubit i. The problem Hamiltonian H_P is given by [34]

$$H_P = \sum_{i,j} J_{ij}\sigma_i^z \cdot \sigma_j^z + \sum_i h_i \sigma_i^z. \tag{5}$$

where σ_i^z is the Pauli-z operator applied to qubit i. The eigenvectors of this Hamiltonian correspond to the solutions of the Ising model (2).

The quantum annealer first initialises the superposition state of a qubit lattice so that $\mathcal{H}(0) = H_I$. The qubit couplings are

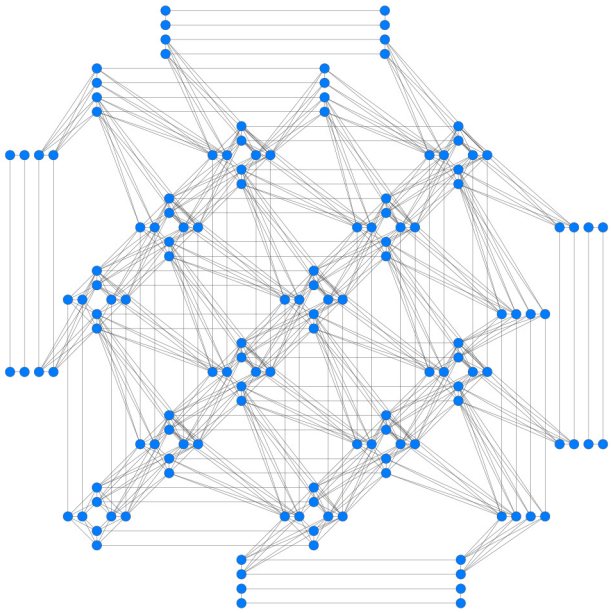

Fig. 1. A 3 by 3 cell example (144 qubits) Pegasus topology. D-Wave's Advantage processor is 16 by 16 cells (5,760 qubits).

then manipulated over the annealing time so that the system evolves towards the problem Hamiltonian. Dwave's device uses radio frequency superconducting quantum–interference device (rf-SQUID) qubits [45]. The underlying physical mechanisms used by D-Wave's quantum processors are described in more detail in [46]. According to the adiabatic theorem of quantum computing, if the annealing time is sufficiently long the time varying Hamiltonian will remain in the ground state throughout. The problem Hamiltonian has classical eigenvalues, and thus the spin values at $\mathcal{H}(1) = H_p$ will be classical values (i.e., $y_i \in \{-1, 1\}$) and these will correspond with the optimal solution of the Ising model.

An added complexity is that the physical qubit lattices within D-Wave's quantum processors are sparsely connected. In September of 2020, D-Wave released its 'Advantage' processor, with 5,760 qubits connected in a Pegasus topology, which has most qubits connected to 15 neighbours. Fig. 1 shows a 144 qubit version of the Pegasus topology [47]. The Advantage processor allows for significantly larger problems than its predecessor, the D-Wave 2000Q, which had 2,048 qubits arranged with most qubits connected to 6 neighbours.

The limited connectivity means that an Ising model must be translated into an equivalent model that is compatible with the processor's physical qubit lattice. The translation process is called minor embedding, and involves representing each logical qubit of the original model with either a single physical qubit or a chain of strongly coupled physical qubits [48]. A example is shown in Fig. 2. Optimal minor embedding is itself a computationally intensive problem, but heuristic tools suitable for large problems have been developed [49]. Also, embeddings can be reused between problems with the same coupled decision variables, even if the linear and quadratic weights are different.

For problems that are too large for current quantum processors, D-Wave makes available cloud-based hybrid solvers,

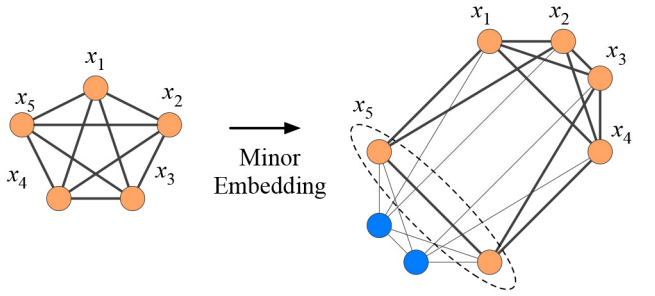

Fig. 2. A 5 qubit logical network representing a simple QUBO problem, $\min\ (x_1 + x_2 + x_3 + x_4 + x_5)^2$, and a 6 qubit embedding on a section of the Pegasus topology.

which can solve QUBO models with up to a million variables [48]. The solver code is proprietary, and is described as making use of parallel computation on classical CPUs and GPUs, which send queries to a quantum processor to help guide the exploration of the solution space [50].

III. Problem Formulation

This section presents the proposed QUBO formulation for a combinatorial OPF problem. To provide a concrete setting, the formulation focuses on a DSO which aims to optimally schedule EVs with controllable on/off charging, while making decisions about the location and sizing of non-dispatchable renewable generation and distribution network upgrades. Note that with fairly minor modifications the formulation could be updated to address transmission networks (e.g., by replacing the distribution-focused multiphase linear power flow model used here [9] with a DC linear power flow model [51]) and a broader range of time-coupled flexible loads, such as smart heating and schedulable appliances [52].

First, a constrained nonlinear binary formulation is presented for the combinatorial problem, which is then used to develop the proposed QUBO formulation, which can be solved using quantum annealing. Consider a distribution network with a set of nodes $\mathcal{N} = \{0, \ldots, N\}$, where node 0 is the point of connection with the main grid. The network has phases $\Phi = \{a, b, c\}$. The set of intervals in the optimisation horizon is $\mathcal{T} = \{1, \ldots, T\}$, where each interval has duration τ. For interval $t \in \mathcal{T}$, the price of energy at the grid connection point is λ_{0t}. $\mathcal{V} = \{1, \ldots, V\}$ is the set of EVs, $\mathcal{G} = \{1, \ldots, G\}$ is the set of potential renewable generation sites and $\mathcal{U} = \{1, \ldots, U\}$ is the set of mutually exclusive potential plans for network upgrades.

The combinatorial OPF includes long-term investment decisions ahead of operation and operational scheduling over the optimisation horizon. Computational limits generally require that the optimisation horizon considers a shortened period representative of longer-term operation (e.g., one or more days). Here, only one set of investment decisions are considered, but a potential extension is to consider multiple stages of investment and operation (e.g., yearly). Due to the difference in timescales, asset investment costs need to be discounted and adjusted based on the duration of the optimisation horizon relative to their lifetime (see, e.g., [53]). The equivalent cost

c_{equ} for the optimisation horizon of an investment with upfront investment cost c_{inv} is given by

$$c_{equ} = c_{inv}\left(\frac{T}{T^y}\right)\left(\frac{r}{1-(1+r)^{-T_L^y}}\right), \tag{6}$$

where T^y is the number of optimisation intervals τ in one year, T_L^y is the asset lifetime in years and r is the discount rate.

For EV $i \in \mathcal{V}$, $\mathcal{T}_i \subseteq \mathcal{T}$ is the subset of intervals when the EV is plugged in and available for charging, $x_{iv}^{ev} \in \{0,1\}$ represents the on/off charging decision for $t \in \mathcal{T}_i$, u_i^{ev} is the utility for energy charged, η_i^{ev} is the charging efficiency, ρ_i^{ev} is the rated charging power, E_{0i}^{ev} is the energy upon arrival, and $\bar{E}_i^{ev}$ is the maximum energy. DERs and loads may have single or multi-phase connections, but for ease of presentation it is assumed that they are wye connected. Ψ_i^v is the set of node–phase pairs which EV i is connected at (e.g., if connected at phases a and b of node n then $\Psi_i^v = \{(n,a),(n,b)\}$).

Each potential renewable generation site $j \in \mathcal{G}$, has a set of sizes $\mathcal{S}_j$ at which generation can be installed, which determine the rated power ρ_{js}^g and cost c_{js}^g, $s \in \mathcal{S}_j$ (discounted and adjusted based on the duration of the optimisation horizon relative to the lifetime). The decision to install generation of size s is indicated by $x_{js}^g \in \{0,1\}$. It is assumed that the renewables sources are non-dispatchable (e.g., solar or wind not controlled by the DSO during operation). Therefore, each source operates with a normalised generation profile over the time horizon, $\hat{p}_j^g = (\hat{p}_{j1}^g, \ldots, \hat{p}_{jT}^g)$, so the total output power vector is $\rho_{js}^g \hat{p}_j^g$.

Using the linear multiphase power flow model from [9] and a set of nominal operating points over the time horizon, time dependent coefficients $A_{\psi\omega t}^{\perp\perp}$ can be obtained relating real power injections at node–phase pair ψ to the change in net real power imports at the slack node. Similarly, a coefficient $K_{\psi\omega t}^{\perp\perp}$ can be obtained which relates the impact of a power injection at node–phase pair ψ to the voltage magnitude of another node–phase pair ω. For node–phase pair ω, let $\tilde{v}_{\omega t}$ be the voltage magnitude at the nominal operating point, with upper and lower allowed limits $\bar{v}_\omega$ and $\underline{v}_\omega$.

The selection of network upgrade plan $k \in \mathcal{U}$ is indicated by $x_k^u \in \{0,1\}$. Plans are mutually exclusive, each being associated with a specific set of upgrades to lines and transformers, resulting in new power flow model coefficients, $A_{\psi kt}^{\perp\perp}$ and $K_{\psi\omega kt}^{\perp\perp}$. The discounted and time horizon adjusted cost of upgrade k is c_k^u. Let $\Delta_{\psi kt}^{A\perp\perp} = A_{\psi kt}^{\perp\perp} - A_{\psi t}^{\perp\perp}$ and $\Delta_{\psi\omega kt}^{K\perp\perp} = K_{\psi\omega kt}^{\perp\perp} - K_{\psi\omega t}^{\perp\perp}$. Also, for time t, let the impact of upgrade k on the net import power at the nominal operating point be given by Δ_{kt}^{p0} and let the impact on the voltage magnitude at node–phase pair ω be given by $\Delta_{\omega kt}^{v}$.

The combinatorial optimisation problem can be formulated as

$$\begin{aligned}
\min\ & \sum_{i\in\mathcal{V}} \frac{1}{|\Psi_i^{ev}|} \sum_{\psi\in\Psi_i^{ev}} \sum_{t\in\mathcal{T}_i} \left(A_{\psi t}^{\perp\perp} + \sum_{k\in\mathcal{U}} \Delta_{\psi kt}^{A\perp\perp} x_k^u\right) \\
& \cdot \tau\lambda_{0t}\eta_i^{ev}\rho_i^{ev}x_{it}^{ev} - \sum_{j\in\mathcal{G}} \frac{1}{|\Psi_j^g|} \sum_{\psi\in\Psi_j^g} \sum_{t\in\mathcal{T}} \\
& \left(A_{\psi t}^{\perp\perp} + \sum_{k\in\mathcal{U}} \Delta_{\psi kt}^{A\perp\perp} x_k^u\right) \sum_{s\in\mathcal{S}_j} x_{js}^g \tau\lambda_{0t}\rho_{js}^g \hat{p}_{jt}^g \\
& - \sum_{i\in\mathcal{V}} \sum_{t\in\mathcal{T}_i} \tau\eta_i^{ev}u_i^{ev}\rho_i^{ev}x_{it}^{ev} + \sum_{j\in\mathcal{G}} \sum_{s\in\mathcal{S}_j} c_{js}^g x_{js}^g \\
& + \sum_{k\in\mathcal{U}} c_k^u x_k^u + \sum_{t\in\mathcal{T}} \tau\lambda_{0t}\Delta_{kt}^{p0} x_k^u, \qquad (7a)
\end{aligned}$$

$$\text{s.t.}\quad E_{0i}^{ev} + \sum_{t\in\mathcal{T}_i} \tau\eta_i^{ev}\rho_i^{ev}x_{it}^{ev} \le \bar{E}_i^{ev} \ \text{ for } i \in \mathcal{V}, \qquad (7b)$$

$$\begin{aligned}
& \underline{v}_\omega \le \tilde{v}_{\omega t} + \sum_{i\in\mathcal{V}} \frac{1}{|\Psi_i^{ev}|} \sum_{\psi\in\Psi_i^{ev}} \rho_i^{ev} \\
& \cdot \left(K_{\psi\omega t}^{\perp\perp} + \sum_{k\in\mathcal{U}} \Delta_{\psi\omega kt}^{K\perp\perp} x_k^u\right) x_{it}^{ev} + \sum_{k\in\mathcal{U}} \Delta_{\omega kt}^{v} x_k^u \\
& - \sum_{j\in\mathcal{G}} \frac{1}{|\Psi_j^g|} \sum_{\psi\in\Psi_j^g} \rho_{js}^g \left(K_{\psi\omega t}^{\perp\perp} + \sum_{k\in\mathcal{U}} \Delta_{\psi\omega kt}^{K\perp\perp} x_k^u\right) \\
& \cdot \sum_{s\in\mathcal{S}_j} x_{js}^g \hat{p}_{jt}^g \le \bar{v}_\omega \quad \text{for} \quad \omega \in \Omega,\ t \in \mathcal{T}, \qquad (7c)
\end{aligned}$$

$$\sum_{s\in\mathcal{S}} x_{js}^g \le 1 \quad \text{for} \quad j \in \mathcal{G}, \quad \sum_{k\in\mathcal{U}} x_k^u \le 1, \qquad (7d)$$

$$x_{it}^{ev}, x_{js}^g, x_k^u \in \{0,1\}. \qquad (7e)$$

The decision variables are x_{it}^{ev}, x_k^u, x_{js}^g, which are all binary valued.

The objective (7a) is to minimise the net system cost, which includes the cost/revenue of buying/selling energy upstream, the utility obtained from EV charging, the cost of renewable generation investment and the cost of network upgrades. Constraint (7b) limits the maximum energy levels of the EVs. Constraint (7c) limits the maximum and minimum voltage magnitude of each node–phase pair $\omega \in \Omega$. Constraints in (7d) specify that a single installation size can be selected for each renewable generation site and that at most a single network upgrade plan can be selected. Constraint (7e) specifies the decision variables are binary.

The problem must be reformulated as a QUBO for it to be solved using quantum annealing. The objective function of the combinatorial OPF problem (7a) is made up of linear and quadratic terms of the binary decision variables and can therefore be directly incorporated into a QUBO formulation. However, since constraints cannot be directly incorporated, the objective must instead include equivalent penalty terms which are high when constraints are violated and zero for feasible solutions. A general linear inequality constraint of form $Ax \le b$ can enforced through an equivalent penalty term [54],

$$P\left(Ax - b + \delta\sum_{l=0}^{Y-1} 2^l y_l\right)^2, \ \text{with } \delta = \frac{\bar{s}}{2^Y - 1}. \tag{8}$$

P is a penalty scalar, which will ensure the constraint is satisfied at optimality if sufficiently large, although an overly large penalty can increase the solution time. Trade-offs and rules-of-thumb for penalty selection are discussed in [54]. Auxiliary slack variables $y_l \in \{0,1\}$, $l \in \{0,\ldots,Y-1\}$ are introduced to enforce inequality, as opposed to equality. These are arranged as a binary expansion, which efficiently enforces the constraint with conservativeness no greater than δ, given that the required slack quantity is no greater than $\bar{s}$.

For specific linear constraints, simpler equivalent penalty terms are available which make use of the properties of binary variables. In particular, for $x_i \in \{0,1\}, i \in \mathcal{N} = \{1,\dots,N\}$, a linear constraint $\sum_{i\in\mathcal{N}} x_i \leq 1$ can be enforced with the following penalty [54],

$$P\sum_{i,j\in\mathcal{N},i\neq j} x_i x_j \tag{9}$$

Due to the network upgrades, (7) also has quadratic inequality constraints. To integrate these into a QUBO, the following penalty term is proposed to enforce the relationship $z = xy$ between $x, y, z \in \{0,1\}$,

$$P(xy - 2zx - 2zy + 3z) \tag{10}$$

This penalty will be 0 if $z = xy$, and greater than or equal to P otherwise.

Using (8), the inequality constraints enforcing the EV maximum energy levels (7b) can be incorporated into the QUBO problem using equivalent penalty terms given by

$$P_{ev}\sum_{i\in\mathcal{V}}\left(E^{ev}_{0i} - \bar{E}^{ev}_{i} + \sum_{t\in\mathcal{T}_i}\tau\eta^{ev}_i\rho^{ev}_i x^{ev}_{it} + \delta^{ev}_i\sum_{l=0}^{Y^{ev}-1}2^l y^{ev}_{il}\right)^2. \tag{11}$$

P_{ev} is the penalty scalar and $y^{ev}_{il} \in \{0,1\}, l \in \{0,\dots,Y^{ev}-1\}$ are binary auxiliary slack variables which enforce the constraint as an inequality. δ^{ev}_i is the maximum conservativeness of the constraint.

The maximum voltage magnitude constraints for each node–phase pair in (7c) can be similarly enforced using equivalent penalty terms given by

$$\begin{aligned}P_v\sum_{t\in\mathcal{T}}\sum_{\omega\in\Omega}\Bigg(&\tilde{v}_{\omega t} - \bar{v}_\omega + \sum_{i\in\mathcal{V}}\frac{1}{|\Psi^{ev}_i|}\sum_{\psi\in\Psi^{ev}_i}\sum_{t\in\mathcal{T}_i}\\ &\rho^{ev}_t\left(K^{\curlywedge}_{\psi\omega t}x^{ev}_{it} + \sum_{k\in\mathcal{U}}\Delta^{K\curlywedge}_{\psi\omega kt}x^{u,ev}_{kit}\right) + \sum_{k\in\mathcal{U}}\Delta^{v}_{\omega kt}x^{u}_{k}\\ &- \sum_{j\in\mathcal{G}}\frac{1}{|\Psi^{g}_j|}\sum_{\psi\in\Psi^{g}_j}\sum_{s\in\mathcal{S}_j}\left(K^{\curlywedge}_{\psi\omega t}x^{g}_{js} + \sum_{k\in\mathcal{U}}\Delta^{K\curlywedge}_{\psi\omega kt}x^{u,g}_{kjs}\right)\\ &\cdot\sum_{t\in\mathcal{T}}\rho^{g}_{js}\hat{p}^{g}_{jt} - \delta^{v}_{\omega t}\sum_{l=0}^{Y^{v}-1}2^l y^{\bar{v}}_{\omega tl}\Bigg)^2.\end{aligned} \tag{12}$$

P_v is the penalty scalar, $y^{\bar{v}}_{\omega tl} \in \{0,1\}, l \in \{0,\dots,Y^{v}-1\}$ are auxiliary slack variables which enforce the constraint as an inequality, and $\delta^{v}_{\omega t}$ is the maximum constraint conservativeness. $x^{u,ev}_{kit}$ and $x^{u,g}_{kjs}$ are binary auxiliary variables, which are introduced to manage the quadratic terms in (7c). Using (10), the required relationships $x^{u,ev}_{kit} = x^{u}_{k}x^{ev}_{it}$ and $x^{u,g}_{kjs} = x^{u}_{k}x^{g}_{js}$ can be enforced by introducing additional penalty terms given by

$$\begin{aligned}&P_{u,ev}\sum_{k\in\mathcal{U}}\sum_{i\in\mathcal{V}}\sum_{t\in\mathcal{T}_i}\left(x^{ev}_{it}x^{u}_{k} - 2x^{ev}_{it}x^{u,ev}_{kit} - 2x^{u}_{k}x^{u,ev}_{kit} - 3x^{u,ev}_{kit}\right)\\ &+P_{u,g}\sum_{k\in\mathcal{U}}\sum_{j\in\mathcal{G}}\sum_{s\in\mathcal{S}j}\left(x^{g}_{js}x^{u}_{k} - 2x^{g}_{js}x^{u,g}_{kjs} - 2x^{u}_{k}x^{u,g}_{kjs} - 3x^{u,g}_{kjs}\right),\end{aligned} \tag{13}$$

where $P_{u,ev}$ and $P_{u,g}$ are the penalty scalars.

Equivalent penalty terms for the minimum voltage magnitude constraints in (7c) are given by

$$\begin{aligned}P_v\sum_{t\in\mathcal{T}}\sum_{\omega\in\Omega}\Bigg(&\tilde{v}_{\omega t} - \underline{v}_\omega + \sum_{i\in\mathcal{V}}\frac{1}{|\Psi^{ev}_i|}\sum_{\psi\in\Psi^{ev}_i}\sum_{t\in\mathcal{T}_i}\\ &\rho^{ev}_t\left(K^{\curlywedge}_{\psi\omega t}x^{ev}_{it} + \sum_{k\in\mathcal{U}}\Delta^{K\curlywedge}_{\psi\omega kt}x^{u,ev}_{kit}\right) + \sum_{k\in\mathcal{U}}\Delta^{v}_{\omega kt}x^{u}_{k}\\ &- \sum_{j\in\mathcal{G}}\frac{1}{|\Psi^{g}_j|}\sum_{\psi\in\Psi^{g}_j}\sum_{s\in\mathcal{S}_j}\left(K^{\curlywedge}_{\psi\omega t}x^{g}_{js} + \sum_{k\in\mathcal{U}}\Delta^{K\curlywedge}_{\psi\omega kt}x^{u,g}_{kjs}\right)\\ &\cdot\sum_{t\in\mathcal{T}}\rho^{g}_{js}\hat{p}^{g}_{jt} - \delta^{v}_{\omega t}\sum_{l=0}^{Y^{v}-1}2^l y^{\underline{v}}_{\omega tl}\Bigg)^2\end{aligned} \tag{14}$$

$y^{\underline{v}}_{\omega tl} \in \{0,1\}, l \in \{0,\dots,Y^{v}-1\}$ are the auxiliary slack variables. Since the maximum and minimum voltage limits have similar characteristics, the same penalty scalar, number of auxiliary variables, and conservativeness parameter are used for both.

Finally, using (9), equivalent penalty terms for the constraints in (7d) specifying that a single installation size can be selected for each renewable generation site, and that a single network upgrade plan can be selected, are given by

$$P_g\sum_{j\in\mathcal{G}}\sum_{s,s'\in\mathcal{S},s\neq s'}x^{g}_{js}x^{g}_{js'} + P_u\sum_{k,k'\in\mathcal{U},k\neq k'}x^{u}_{k}x^{u}_{k'}, \tag{15}$$

where P_g and P_u are the penalty scalars.

Bringing together the original objective function (7a) and the equivalent penalty terms for constraint enforcement (11)–(15), the proposed equivalent QUBO formulation for (7) is given by

$$\min \quad (7a) + (11) + (12) + (13) + (14) + (15).$$

The QUBO problem has decision variables x^{ev}_{it}, x^{u}_{k}, x^{g}_{js}, $x^{u,ev}_{kit}$, $x^{u,g}_{kjs}$, y^{ev}_{il}, $y^{\bar{v}}_{\omega tl}$, $y^{\underline{v}}_{\omega tl}$, which are all binary valued.

The proposed formulation focuses on DERs with discrete flexibility, which require combinatorial optimisation. The formulation could be extended to also include continuously controllable DERs based on a small discrete control step-size and continuous output powers approximated by multiple binary decision variables (arranged in binary expansions). For example, consider a controllable generation source with output power p^c_t, limited by $0 \leq p^c_t \leq \bar{p}^c$. Let the control step-size be δ^c and the additional binary decision variables be $x^c_{tm} \in \{0,1\}, m \in \{0,\dots,N^c-1\}$, where $N^c = \text{ceil}\{\log_2(\bar{p}^c/\delta^c)\}$. The DER's output power would be $p^c_t = \delta^c\sum_{m=0}^{N^c-1}2^m x^c_{tm}$, which could be incorporated into the objective and penalty terms of the QUBO problem.

IV. Case Studies

In this section, case studies are presented demonstrating the implementation of the proposed QUBO formulation. The case studies make use the IEEE European Low Voltage Test Feeder [55], shown in Fig. 3, with controllable on/off EV

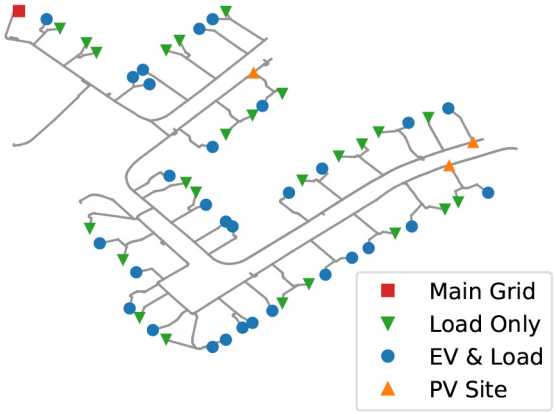

Fig. 3. The distribution feeder used for the case studies, showing the location of the main grid connection, 55 domestic loads, 30 of which may have EV charging, and 3 sites where PV generation can be installed.

charging, photovoltaic (PV) generation placement/sizing and network upgrade decisions.

The network has 55 single phase domestic loads, and up to 30 EVs with single phase 7.2 kW chargers and batteries sizes of 75, 85 or 100 kWh. The EV arrival and departure times are normally distributed. The mean arrival time is 6 pm and mean departure time is 8 am, both with a standard deviation of 2 h. The EVs' energy upon arrival is uniformly distributed between 10% and 30%. The network has 3 PV generation sites which have three phase connections and can support 25 or 50 kWp. Two network upgrade plans are available, which respectively reduce the impedance of the transformers and lines by half or three quarters. The case studies consider a 24 hour optimisation horizon from 12 pm to 12 pm the next day, with 1 h duration intervals.

Here, operation over a single day with 1 h intervals has been chosen since the focus is demonstrating the implementability of the proposed QUBO formulation, but it could be refined by considering multiple representative days and more granular scheduling (at the cost of increased computational burden). The upstream energy price is assumed to follow a standard U.K. 'Economy 7' tariff, with an energy price of £0.15 / kWh from 6 am to 11 pm and £0.07 / kWh from 11 pm to 6 am [56]. Smart meter data from the U.K. Customer-Led Network Revolution project is used for the domestic loads [57]. Scale-dependent PV installation costs are calculated using data from [58], assuming a 25-year lifetime and 5% discount rate. The network upgrade costs are calculated using data from [59], assuming a 35-year lifetime and 5% discount rate. The voltage magnitude limits are assumed to be 0.95 and 1.05 pu. Additional case study parameters are provided in Table I.

TABLE I
ADDITIONAL CASE STUDY PARAMETERS

u_i^{ev}	0.50	£/kWh	η_i^{ev}	90	%
c_{1j}^{g}	8.42	£	c_{2j}^{g}	16.41	£
c_1^u	26.32	£	c_2^u	78.96	£
P_{ev}	0.5		Y_{ev}	4	
δ_i^{ev}	6	kWh	P_v	2	
Y_v	5		$\delta_{\omega t}^{v}$	0.003	pu
P_g	240		P_u	300	
$P_{u,ev}$	10		$P_{u,g}$	240	

A. Quantum Processor Implementation

The proposed QUBO problem is implemented on D-Wave's 5,760 qubit Advantage quantum processor to investigate how the number of required qubits scales with the problem size. To do this, the problem is implemented for different numbers of EVs and node–phase pairs where the upper and lower voltage limits are enforced. Adding additional EVs increases the number of decision variables (EV charging decisions over the time horizon, EV energy constraint slack variables, and auxiliary variables associated with network upgrades), and adds new quadratic relationships between variables, which may also add qubits to enable minor embedding on the Pegasus topology. Adding additional voltage constraints similarly increases the number of decision variables and quadratic relationships.

When implemented with a single EV and voltage limits on 3 node–phase pairs without including network upgrades, the QUBO formulation has 746 decision variables. This increases to 792 when network upgrade decisions are included. Given voltage limits on 3 node–phase pairs, without network upgrades each additional EV adds on average 17 decision variables to the problem, while with network upgrades extra EVs add an average of 44 decision variables (note that the number of extra decision variables varies depending on the number of intervals each EV is available for charging). Given a single EV, enforcing voltage limits at an additional node–phase pair increases the number of decision variables by 240, regardless of whether or not network upgrades are considered.

Fig. 4a shows the number of assigned qubits for different numbers of EVs, given voltage limits are enforced at 3 node–phase pairs, and Fig. 4b which shows the number of assigned qubits for a single EV and different numbers of node–phase pairs with voltage limits. For each problem size, the range of assigned qubits provided by D-Wave's heuristic minor embedding tool for 20 runs is shown, varying from the mean by at most ±9.4%. Without including network constraints, the number of assigned qubits increases approximately linearly up to 9 EVs and 8 node–phase pairs with voltage limits, beyond which feasible embeddings are not regularly found. A similar relationship is seen with network upgrades, but feasible embeddings are not regularly found above 5 EVs and 7 node–phase pairs with voltage limits. Linear scaling indicates that the proposed formulation should meaningfully benefit as larger annealing-based quantum processors become available. However, the current maximum problem size is restrictive even for relatively small-scale applications.

To investigate the performance of quantum annealing compared with classical computing, the proposed QUBO problem was solved using D-Wave's Advantage processor and with simulated annealing, which is a state-of-the-art classical method for combinatorial optimization problems [60]. For quantum annealing, the problem was solved using 100 samples and an annealing time of 100 μs. For simulated annealing, the problem was implemented using the dwave-neal Python package [61], and solved using a 2.3 GHz 8-core Intel Core i9

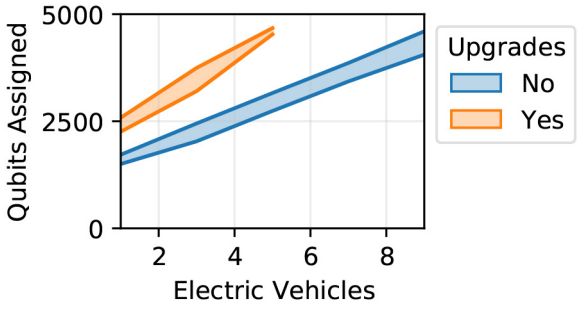

(a)

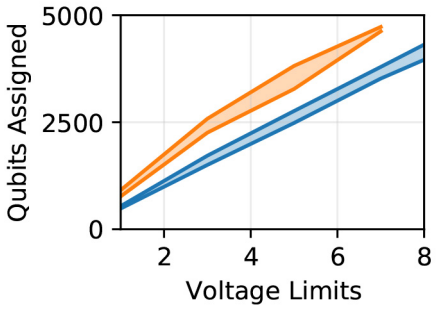

(b)

Fig. 4. The number of assigned qubits on D-Wave's Pegasus topology for (a) different numbers of EVs, given voltage limits at 3 node–phase pairs, and (b) voltage limits enforced at different numbers of node–phase pairs, given a single EV, with and without network upgrade decisions.

processor and 16 GB of RAM. To allow comparison between the computation time of the two methods, simulated annealing was implemented with one repetition and two sweeps, which was found to result in solutions of similar energy (i.e., the QUBO objective including penalty terms). Table II compares the average computation time, average net utility and average energy of the two methods, when the problem is formulated with different numbers of EVs, voltage limits at 3 node–phase pairs and without considering network upgrade decisions. The averages were obtained by solving each formulation 10 times using each method. As shown, for a single EV, quantum annealing has a lower average computation time, higher average net utility and lower average energy. Also, under quantum annealing, the computation time only increases slightly from 49.9 ms with 1 EV, to 52.2 ms with 9 EVs, while the computation time for simulated annealing increases from 56.4 ms to 121.5 ms. The average net utility is also consistently higher using quantum annealing. Each method yields similar average QUBO energies, driven mainly by slight constraint violations. However, for simulated annealing the average energy is more consistent for different problem sizes, while using quantum annealing there is an upward trend with increasing problem size, which could indicate a future scaling challenge.

B. Hybrid Solver Implementation

D-Wave's hybrid quantum-classical binary quadratic model solver allows larger problems of practical interest to be solved. To demonstrate this, case studies are presented with 30 EVs, which together have a significant impact on local power

TABLE II
COMPARISON BETWEEN THE AVERAGE COMPUTATION TIME, AVERAGE NET UTILITY AND AVERAGE QUBO ENERGY, WHEN THE QUBO PROBLEM IS SOLVED 10 TIMES USING SIMULATED ANNEALING (SA) AND QUANTUM ANNEALING (QA). THE QUBO PROBLEM WAS FORMULATED WITH DIFFERENT NUMBERS OF EVS, VOLTAGE LIMITS AT 3 NODE–PHASE PAIRS AND WITHOUT NETWORK UPGRADE DECISIONS

No.	Avg. Time (ms)		Avg. Net Utility (£)		Avg. Energy ($\times 10^3$)	
EVs	SA	QA	SA	QA	SA	QA
1	56.4	49.9	−78.9	−70.4	2.03	1.70
3	84.9	50.0	−47.6	−40.5	2.00	2.24
5	94.9	51.2	−14.1	−4.6	2.15	2.25
7	105.7	51.4	−3.2	13.6	1.91	2.40
9	121.5	52.2	25.5	37.4	2.10	2.47

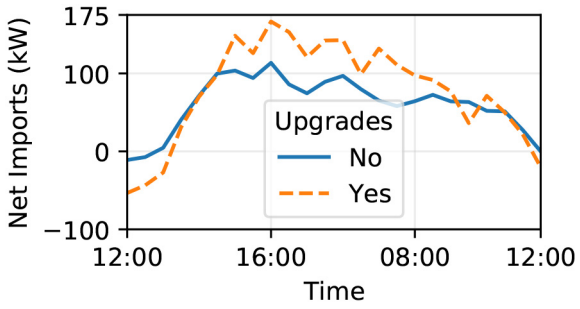

Fig. 5. The net real import power for case studies with 30 EVs, with and without network upgrade decisions, using D-Wave's hybrid binary quadratic solver with a time limit of 120 s.

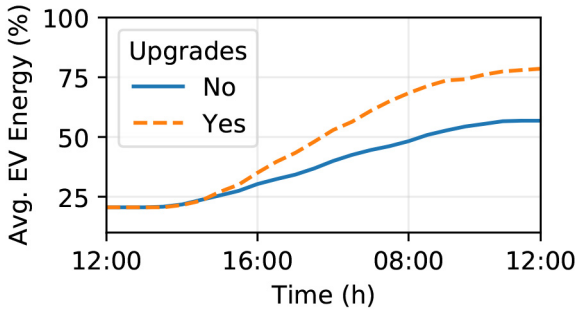

Fig. 6. The average EV energy for case studies with 30 EVs, with and without network upgrade decisions, using D-Wave's hybrid binary quadratic solver with a time limit of 120 s.

demand and network voltages. Upper and lower voltage limits are specified for 12 node–phase pairs spread throughout the network. Case studies with and without the potential for network upgrades are compared to show the additional value of co-optimising operational flexibility and network investment decisions. The hybrid solvers are heuristic, iteratively making use of both classical and quantum computation for a specified time limit, where upon the solution giving the lowest total energy (QUBO objective) is returned.

First, case studies with and without network upgrades are completed with a time limit of 120 s. Fig. 5 shows the net power imported from the main grid for each case, and Fig. 6 shows the average energy of the 30 EVs. Fig. 7 shows the range of the voltage magnitudes across the three phases. In the case where network upgrades are allowed, the solution returned by the hybrid solver specifies the moderate network upgrade plan (reducing impedances by half) and 100 kW of

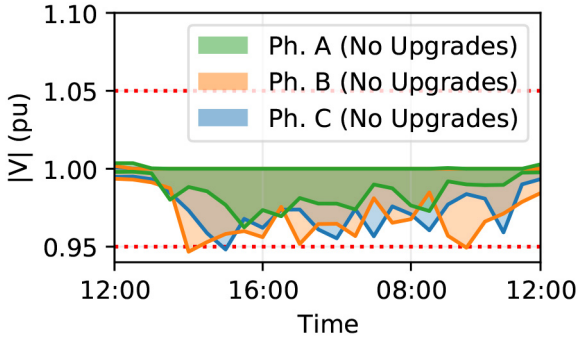

(a)

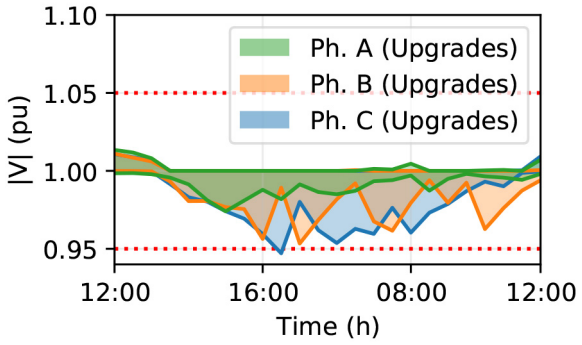

(b)

Fig. 7. The voltage magnitude range across the nodes for each phase for case studies with 30 EVs, using D-Wave's hybrid binary quadratic solver with a time limit of 120 s. The voltage limits are 0.95 pu and 1.05 pu. The voltage magnitude ranges are shown for (a) the case without network upgrade decisions and (b) the case with network upgrade decisions.

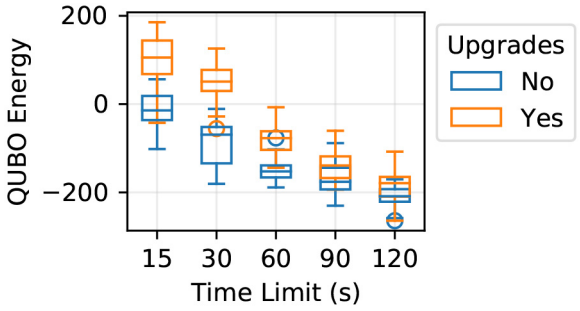

(a)

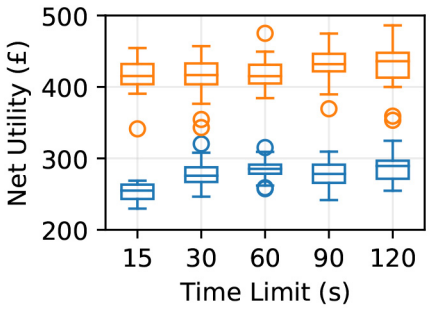

(b)

Fig. 8. Results from solving the QUBO problem 30 times for a range hybrid solver time limits, with and without network upgrade decisions. Distributions are shown for (a) the QUBO energy and (b) net utility values. The box plots show the median (centre line), interquartile range (box), 1.5 times the interquartile range above/below the box (whiskers), and outliers (circles).

PV generation (split between the three potential sites). Without network upgrades, only 50 kW of PV is installed, at the site closest to the main grid.

As shown in Fig. 5, allowing network upgrades results in greater maximum import and export of power, and from Fig. 6 it can be seen that the EVs reach a higher final average energy level (78.6% compared with 56.8%). With network upgrades enabled, the overall net utility over the day is £452, which is 78% higher than the net utility without network upgrades (£254). For the node–phase pairs where the voltage limits are explicitly enforced, the lowest voltage magnitude reached is 0.958 pu for the case without network upgrades, and 0.951 for the case with network upgrades. As seen in Fig. 7(a) and 7(b), there are slight violations at nodes where the limits are not enforced, with 0.947 pu the lowest voltage magnitude reached in both cases.

Next, to show the impact of the hybrid solver time limits, the QUBO problem is solved 30 times for a range limits between 15 s and 120 s, with and without network upgrade decisions. Note that D-Wave's hybrid solver imposes a minimum time limit based on its assessment of the problem complexity, which varied around 12 s, so 15 s was selected as a consistent starting point. The box plots in Fig. 8a and Fig. 8b show the distributions of the QUBO energy (returned objective function value) and net utility. As shown in Fig. 8a, increasing the time limit reduces the QUBO energy, with diminishing returns starting to be seen above 60 s. Most of this reduction results from slight improvements in constraint satisfaction, and from Fig. 8b, it can be seen that the average net utility is fairly stable above 30 s. The heuristic nature of the hybrid solver is clear from the variability of the net utility, but it can be seen that even accounting for outliers, the net utility for cases where network upgrades are allowed is consistently higher than when they are disallowed.

V. Conclusion

Annealing-based quantum computing offers a new computing hardware platform with the future potential to efficiently solve large-scale combinatorial optimisation problems. This could be highly valuable for the power sector, particularly for network operators aiming to integrate DER flexibility into network planning and investment decision making. To demonstrate this opportunity, a novel QUBO formulation which can be solved with quantum annealing was developed for a linear multiphase OPF problem, with controllable on/off EV charging, renewable generation placement/sizing and network upgrade decisions. Case studies based on the IEEE European Low Voltage Test Feeder were implemented on D-Wave's 5,760 qubit Advantage quantum processor to show how the problem size impacts the required number of qubits. Although it was found that the quantum processor is too small for distribution-scale applications, the number of qubits was observed to grow linearly with the number of EVs and the number of network voltage constraints, indicating that there is a promising future opportunity given the rate of technological development of annealing-based quantum processors.

D-Wave's hybrid quantum-classical binary quadratic model solver was also used to solve larger case studies with 30 EVs, where EV charging flexibility has a significant impact on distribution network power flows. In this case, combinatorial co-optimisation of EV flexibility with generation and network investment decisions was shown to offer substantial value. The paper has focused on deterministic combinatorial OPF as a first step, but in practice network planning and scheduling applications may involve significant uncertainty due to the weather-dependence of renewable generation and the behaviour-dependence of flexible loads. An important area for future work is to investigate how methods for robust optimisation (see, e.g., [62]) can be implemented within the qubit limitations of quantum annealers. Another important area for future work is the optimal selection of penalty terms, which are necessary for constraint handling within the proposed formulation, but may affect the computation time and solution quality if chosen inappropriately.

REFERENCES

[1] L. N. Ochoa, F. Pilo, A. Keane, P. Cuffe, and G. Pisano, "Embracing an adaptable, flexible posture: Ensuring that future European distribution networks are ready for more active roles," *IEEE Power Energy Mag.*, vol. 14, no. 5, pp. 16–28, Sep./Oct. 2016.

[2] A. Dimeas *et al.*, "Smart houses in the smart grid: Developing an interactive network," *IEEE Electrific. Mag.*, vol. 2, no. 1, pp. 81–93, Mar. 2014.

[3] F. Alexander *et al.*, "Exascale applications: Skin in the game," *Philos. Trans. Royal Soc. A, Math. Phys. Eng. Sci.*, vol. 378, no. 2166, Mar. 2020, Art. no. 20190056.

[4] H. W. Dommel and W. F. Tinney, "Optimal power flow solutions," *IEEE Trans. Power App. Syst.*, vol. PAS-87, no. 10, pp. 1866–1876, Oct. 1968.

[5] J. Momoh, R. Adapa, and M. El-Hawary, "A review of selected optimal power flow literature to 1993. I. Nonlinear and quadratic programming approaches," *IEEE Trans. Power Syst.*, vol. 14, no. 1, pp. 96–104, Feb. 1999.

[6] J. Lavaei and S. H. Low, "Zero duality gap in optimal power flow problem," *IEEE Trans. Power Syst.*, vol. 27, no. 1, pp. 92–107, Feb. 2012.

[7] S. Gill, I. Kockar, and G. W. Ault, "Dynamic optimal power flow for active distribution networks," *IEEE Trans. Power Syst.*, vol. 29, no. 1, pp. 121–131, Jan. 2014.

[8] L. Gan, N. Li, U. Topcu, and S. H. Low, "Exact convex relaxation of optimal power flow in radial networks," *IEEE Trans. Autom. Control*, vol. 60, no. 1, pp. 72–87, Jan. 2015.

[9] A. Bernstein, C. Wang, E. DallAnese, J.-Y. Le Boudec, and C. Zhao, "Load Flow in multiphase distribution networks: Existence, uniqueness, non-singularity and linear models," *IEEE Trans. Power Syst.*, vol. 33, no. 6, pp. 5832–5843, Nov. 2018.

[10] M. Khonji, S. C. K. Chau, and K. Elbassioni, "Combinatorial optimization of AC optimal power flow with discrete demands in radial networks," *IEEE Trans. Control Netw. Syst.*, vol. 7, no. 2, pp. 887–898, Jun. 2020.

[11] D. Ernst, M. Glavic, G. Stan, S. Mannor, and L. Wehenkel, "The cross-entropy method for power system combinatorial optimization problems," in *Proc. IEEE Lausanne Power Tech*, Jul. 2007, pp. 1290–1295.

[12] B. Sun, Z. Huang, X. Tan, and D. H. K. Tsang, "Optimal scheduling for electric vehicle charging with discrete charging levels in distribution grid," *IEEE Trans. Smart Grid*, vol. 9, no. 2, pp. 624–634, Mar. 2018.

[13] M. Zhang, Q. Wu, T. B. H. Rasmussen, X. Yang, and J. Wen, "Heat pumps in Denmark: Current situation of providing frequency control ancillary services," *CSEE J. Power Energy Syst.*, vol. 8, no. 3, pp. 769–779, May 2022.

[14] D. Papadaskalopoulos and G. Strbac, "Nonlinear and randomized pricing for distributed management of flexible loads," *IEEE Trans. Smart Grid*, vol. 7, no. 2, pp. 1137–1146, Mar. 2016.

[15] C. Crozier, M. Deakin, T. Morstyn, and M. McCulloch, "Incorporating charger efficiency into electric vehicle charging optimization," in *Proc. IEEE PES Innov. Smart Grid Technol. Europe (ISGT-Europe)*, Sep. 2019, pp. 1–5.

[16] D. Apostolopoulou, S. Bahramirad, and A. Khodaei, "The interface of power: Moving toward distribution system operators," *IEEE Power Energy Mag.*, vol. 14, no. 3, pp. 46–51, Jun. 2016.

[17] P. S. Georgilakis and N. D. Hatziargyriou, "Optimal distributed generation placement in power distribution networks: Models, methods, and future research," *IEEE Trans. Power Syst.*, vol. 28, no. 3, pp. 3420–3428, Aug. 2013.

[18] P. You, Z. Yang, M.-Y. Chow, and Y. Sun, "Optimal cooperative charging strategy for a smart charging station of electric vehicles," *IEEE Trans. Power Syst.*, vol. 31, no. 4, pp. 2946–2956, Jul. 2016.

[19] L. Liberti, "Undecidability and hardness in mixed-integer nonlinear programming," *RAIRO Oper. Res.*, vol. 53, no. 1, pp. 81–109, Jan. 2019.

[20] X. Zhao, P. B. Luh, and J. Wang, "Surrogate gradient algorithm for lagrangian relaxation," *J. Optim. Theory Appl.*, vol. 100, no. 3, pp. 699–712, Mar. 1999.

[21] M. L. Fisher, "The Lagrangian relaxation method for solving integer programming problems," *Manage. Sci.*, vol. 50, no. 12S, pp. 1861–1871, Dec. 2004.

[22] S. Zhou *et al.*, "The combinatorial optimization by genetic algorithm and neural network for energy storage system in solar energy electric vehicle", *Proc. World Congr. Intell. Control Autom. (WCICA)*, pp. 2838–2842, Jun. 2008, doi: 10.1109/WCICA.2008.4593375.

[23] J. Soares, Z. Vale, B. Canizes, and H. Morais, "Multi-objective parallel particle swarm optimization for day-ahead vehicle-to-grid scheduling," in *Proc. IEEE Symp. Comput. Intell. Appl. Smart Grid*, 2013, pp. 138–145.

[24] H. Mori and S. Sudo, "Strategic tabu search for unit commitment in power systems," *IFAC Proc. Vol.*, vol. 36, no. 20, pp. 485–490, Sep. 2003.

[25] N. Deeb, "Simulated annealing in power systems," in *Proc. IEEE Int. Conf. Syst. Man Cybern.*, Jan. 1992, pp. 1086–1089.

[26] S. Chen, J. Montgomery, and A. Bolufé-Röhler, "Measuring the curse of dimensionality and its effects on particle swarm optimization and differential evolution," *Appl. Intell.*, vol. 42, no. 3, pp. 514–526, Apr. 2015.

[27] F. Arute *et al.*, "Quantum supremacy using a programmable superconducting processor," *Nature*, vol. 574, no. 7779, pp. 505–510, Oct. 2019.

[28] F. Feng, P. Zhang, M. A. Bragin, and Y. Zhou, "Novel resolution of unit commitment problems through quantum surrogate Lagrangian relaxation," *IEEE Trans. Power Syst.*, early access, Jun. 10, 2022, doi: 10.1109/TPWRS.2022.3181221.

[29] N. Nikmehr, P. Zhang, and M. A. Bragin, "Quantum distributed unit commitment," *IEEE Trans. Power Syst.*, vol. 37, no. 5, pp. 3592–3603, Sep. 2022.

[30] J. Preskill, "Quantum computing in the NISQ era and beyond," *Quantum*, vol. 2, p. 79, Aug. 2018.

[31] P. Hauke, H. G. Katzgraber, W. Lechner, H. Nishimori, and W. D. Oliver, "Perspectives of quantum annealing: Methods and implementations," *Rep. Progr. Phys.*, vol. 83, no. 5, May 2020, Art. no. 54401.

[32] S. E. Venegas-Andraca, W. Cruz-Santos, C. McGeoch, and M. Lanzagorta, "A cross-disciplinary introduction to quantum annealing-based algorithms," *Contemp. Phys.*, vol. 59, no. 2, pp. 174–197, 2018.

[33] T. Kadowaki and H. Nishimori, "Quantum annealing in the transverse ising model," *Phys. Rev. E, Stat. Phys. Plasmas Fluids Relat. Interdiscip. Top.*, vol. 58, no. 5, pp. 5355–5363, Nov. 1998.

[34] C. C. McGeoch, "Theory versus practice in annealing-based quantum computing," *Theor. Comput. Sci.*, vol. 816, pp. 169–183, Jan. 2020.

[35] T. Albash and D. A. Lidar, "Demonstration of a scaling advantage for a quantum annealer over simulated annealing," *Phys. Rev. X*, vol. 8, no. 3, Jul. 2018, Art. no. 31016. [Online]. Available: https://link.aps.org/doi/10.1103/PhysRevX.8.031016

[36] A. D. King *et al.*, "Scaling advantage over path-integral Monte Carlo in quantum simulation of geometrically frustrated magnets," *Nat. Commun.*, vol. 12, no. 1, pp. 1–6, Feb. 2021.

[37] E. J. Crosson and D. A. Lidar, "Prospects for quantum enhancement with diabatic quantum annealing," *Nat. Rev. Phys.*, vol. 3, no. 7, pp. 466–489, Jul. 2021.

[38] A. Perdomo-Ortiz, N. Dickson, M. Drew-Brook, G. Rose, and A. Aspuru-Guzik, "Finding low-energy conformations of lattice protein models by quantum annealing," *Sci. Rep.*, vol. 2, pp. 1–7, Aug. 2012.

[39] J. Biamonte, P. Wittek, N. Pancotti, P. Rebentrost, N. Wiebe, and S. Lloyd, "Quantum machine learning," *Nature*, vol. 549, no. 7671, pp. 195–202, 2017.

[40] M. Kim, D. Venturelli, and K. Jamieson, "Leveraging quantum annealing for large MIMO processing in centralized radio access networks," in *Proc. Conf. ACM Special Interest Group Data Commun.*, 2019, pp. 241–255.

[41] R. Eskandarpour, K. J. B. Ghosh, A. Khodaei, A. Paaso, and L. Zhang, "Quantum-enhanced grid of the future: A primer," *IEEE Access*, vol. 8, pp. 188993–189002, 2020.
[42] A. Ajagekar and F. You, "Quantum computing for energy systems optimization: Challenges and opportunities," *Energy*, vol. 179, no. 607, pp. 76–89, Jul. 2019.
[43] D. Wang, K. Zheng, Q. Chen, Z. Li, and S. Liu, "Quantum annealing computing for grid partition in large-scale power systems," in *Proc. IEEE 5th Int. Electr. Energy Conf. (CIEEC)*, 2022, pp. 2004–2009.
[44] E. B. Jones *et al.*, "On the computational viability of quantum optimization for PMU placement," in *Proc. IEEE Power Energy Soc. Gen. Meeting (PESGM)*, 2020, pp. 1–5.
[45] M. Kjaergaard *et al.*, "Superconducting qubits: Current state of play," *Annu. Rev. Condens. Matter Phys.*, vol. 11, no. 1, pp. 369–395, Mar. 2020.
[46] R. Harris *et al.*, "Experimental demonstration of a robust and scalable flux qubit," *Phys. Rev. B, Condens. Matter Condens. Matter Mater. Phys.*, vol. 81, no. 13, pp. 1–20, Apr. 2010.
[47] K. Boothby, P. Bunyk, J. Raymond, and A. Roy, "Next-generation topology of D-wave quantum processors," D-Wave Technical Report Series, D-Wave Syst., Burnaby, BC, Canada, Rep. 14-1026A-C, 2020. [Online]. Available: dwavesys.com/learn/publications
[48] C. McGeoch and P. Farré, "The D-Wave advantage system: An overview," D-Wave Technical Report Series, D-Wave Syst., Burnaby, BC, Canada, Rep. 14-1049A-A, 2020. [Online]. Available: dwavesys.com/learn/publications
[49] Y. Sugie *et al.*, "Minor-embedding heuristics for large-scale annealing processors with sparse hardware graphs of up to 102,400 nodes," *Soft Comput.*, vol. 25, no. 3, pp. 1731–1749, 2021.
[50] W. Bernoudy, C. Mcgeoch, and P. Farr, "D-Wave hybrid solver service + advantage: Technology update," D-Wave Technical Report Series, D-Wave Syst., Burnaby, BC, Canada, Rep. 14-1048A-A, 2020. [Online]. Available: dwavesys.com/learn/publications
[51] B. Stott, J. Jardim, and O. Alsaç, "DC power flow revisited," *IEEE Trans. Power Syst.*, vol. 24, no. 3, pp. 1290–1300, Aug. 2009.
[52] L. Barth, N. Ludwig, E. Mengelkamp, and P. Staudt, "A comprehensive modelling framework for demand side flexibility in smart grids," *Comput. Sci. Res. Develop.*, vol. 33, nos. 1–2, pp. 13–23, Feb. 2018.
[53] C. Huang, C. Wang, N. Xie, and Y. Wang,, "Robust coordination expansion planning for active distribution network in deregulated retail power market," *IEEE Trans. Smart Grid*, vol. 11, no. 2, pp. 1476–1488, Mar. 2020.
[54] F. Glover, G. Kochenberger, and Y. Du, "Quantum bridge analytics I: A tutorial on formulating and using QUBO models," *4OR*, vol. 17, no. 4, pp. 335–371, Dec. 2019.
[55] "European low voltage test feeder." Accessed: Feb. 1, 2022. [Online]. Available: cmte.ieee.org/pes-testfeeders
[56] "A complete guide to economy 7 and how it works." Accessed: Feb. 1, 2022. [Online]. Available: uswitch.com/gas-electricity/guides/economy-7
[57] "Enhanced profiling of domestic customers with solar photovoltaics." Customer-Led Network Revolution. Accessed: Feb. 1, 2022. [Online]. Available: networkrevolution.co.uk
[58] D. Feldman, V. Ramasamy, R. Fu, A. Ramdas, J. Desai, and R. Margolis, "U.S. solar photovoltaic system and energy storage cost benchmark: Q1 2020," Nat. Renew. Energy Lab., Golden, CO, USA, Rep. NREL/TP-6A20-77324, Sep. 2021.
[59] D. Cartlidge, *Spon's Mechanical and Electrical Services Price Book*. Boca Raton, FL, USA: CRC Press, 2018.
[60] S. V. Isakov, I. N. Zintchenko, T. F. Rønnow, and M. Troyer, "Optimised simulated annealing for Ising spin glasses," *Comput. Phys. Commun.*, vol. 192, pp. 265–271, Jul. 2015.
[61] "Dwave-neal documentation." D-Wave Systems. 2022. [Online]. Available: docs.ocean.dwavesys.com
[62] D. Bertsimas, D. B. Brown, and C. Caramanis, "Theory and applications of robust optimization," *SIAM Rev.*, vol. 53, no. 3, pp. 464–501, 2011.

Thomas Morstyn (Senior Member, IEEE) received the B.Eng. degree (Hon.) in electrical engineering from the University of Melbourne in 2011, and the Ph.D. degree in electrical engineering from the University of New South Wales in 2016.

He is a Lecturer of Power Electronics and Smart Grids with the School of Engineering, University of Edinburgh. He is also the Deputy Champion of Energy Distribution and Infrastructure for the Scottish Energy Technology Partnership. His research interests include multi-agent control and market design for integrating distributed energy resources into power system operations. He is an Associate Editor of IEEE TRANSACTIONS ON POWER SYSTEMS.